Cellular/Molecular

Differential Somatic Ca^{2+} Channel Profile in Midbrain Dopaminergic Neurons

Fabian Philippart,[1] Geoffrey Destreel,[1] Paulina Merino-Sepúlveda,[2] Pablo Henny,[2] Dominique Engel,[1]* and Vincent Seutin[1]*

[1]Neurophysiology Unit, GIGA Neurosciences, University of Liège, B-4000 Liège, Belgium, and [2]Departamento de Anatomía Normal, Escuela de Medicina, and Centro Interdisciplinario de Neurociencias, Pontificia Universidad Católica de Chile, Santiago, Chile

Dopaminergic (DA) neurons located in the ventral midbrain continuously generate a slow endogenous pacemaker activity, the mechanism of which is still debated. It has been suggested that, in the substantia nigra pars compacta (SNc), the pacemaking relies more on Ca^{2+} channels and that the density of L-type Ca^{2+} channels is higher in these DA neurons than in those located in the ventral tegmental area (VTA). This might lead to a higher Ca^{2+} load in SNc DA neurons and explain their higher susceptibility to degeneration. However, direct evidence for this hypothesis is lacking. We found that the L-type current and channel density are indeed higher in the somata of rat SNc DA neurons and that this current undergoes less inactivation in this region. Nonstationary fluctuation analysis measurements showed a much higher number of L-type channels in the soma of SNc DA neurons, as well as a smaller single-channel conductance, pointing to a possible different molecular identity of L-type channels in DA neurons from the two areas. A major consequence of this is that pacemaking and, even more so, bursting are associated with a larger Ca^{2+} entry through L-type channels in SNc DA neurons than in their VTA counterparts. Our results establish a molecular and functional difference between two populations of midbrain DA neurons that may contribute to their differential sensitivity to neurodegeneration.

Key words: **action potential clamp; dopaminergic neurons; neurodegeneration; nonstationary fluctuation analysis; nucleated patches; voltage-dependent calcium channels**

Significance Statement

Dopamine neurons from the substantia nigra pars compacta (SNc) and ventral tegmental area (VTA) are involved in various brain functions, such as movement initiation and goal directed behavior, respectively. This work shows that, although both neurons fire in a similar regular and slow pacemaker mode, this firing activity is supported by different calcium channel landscapes. Indeed, the L-type calcium current is larger in the soma of dopamine neurons of the SNc, leading to a higher charge transfer through L-type channels during pacemaking and bursting. Therefore, these neurons may be physiologically exposed to a larger stress than their neighbors from the VTA.

Introduction

The electrical phenotype of neurons is extraordinarily diverse, with major differences in ion channel density and topography throughout the somatic, dendritic, and axonal compartments among different types of neurons (Magee, 1999). These features underlie various properties of neurons, such as their ability to generate pacemaker activity and the extent of backpropagation of action potentials within the somatodendritic compartment (Häusser et al., 1995). In addition, it is possible that differences in ion channel buildup underlie the propensity of some neuronal populations to degenerate in pathological conditions (Bernard and Shevell, 2008).

Dopaminergic (DA) neurons are slow pacemaker neurons located mostly in the midbrain. They play a key role in many different brain functions, such as the control of movement, reward, motivation, and cognition (Nieoullon, 2002; Wise, 2004; Fields et

Received Feb. 10, 2016; revised May 6, 2016; accepted May 31, 2016.

Author contributions: F.P., P.H., D.E., and V.S. designed research; F.P., G.D., P.M.-S., and P.H. performed research; F.P., D.E., and V.S. analyzed data; F.P. and V.S. wrote the paper.

This work was supported by Fonds National de la Recherche Scientifique (Belgium) Grant T.0015.13 to V.S. and D.E. and Belgian Science Policy (Interuniversity Attraction Poles Program Grant P7/10 to V.S. P.H. was supported by grants 1141170 from FONDECYT, Chile and ACT-1109 from Anillo-CONICYT, Chile. We thank Laurent Massotte and Christelle Gillissen for technical assistance; the GIGA Imaging platform (Dr. Sandra Ormenese) for their help with the imaging; and Drs. Guillaume Drion, Neil Marrion, and Joerg Striessnig for helpful discussions on the manuscript.

The authors declare no competing financial interests.

*D.E. and V.S. contributed equally to this study.

Correspondence should be addressed to Dr. Vincent Seutin, University of Liège, Laboratory of Pharmacology and GIGA Neurosciences, University Hospital (B36), Quartier Hôpital, Avenue Hippocrate 15, 4000 Liège, Belgium. E-mail: V.Seutin@ulg.ac.be.

DOI:10.1523/JNEUROSCI.0459-16.2016

 0270-6474/16/367234-12$15.00/0

al., 2007; Schultz, 2007). Several populations of midbrain DA neurons have been identified, each having specific projections and/or electrophysiological properties (Cameron et al., 1997; Neuhoff et al., 2002; Wolfart and Roeper, 2002; Lammel et al., 2008; Liss and Roeper, 2008; Margolis et al., 2008). In addition, transcriptomic profiles of DA neurons also are heterogeneous (Grimm et al., 2004; Chung et al., 2005; Poulin et al., 2014). Despite their differences, a majority of DA neurons share the ability to fire spontaneously at slow rates in the absence of excitatory input. This pacemaker activity is believed to be responsible for the control of the basal concentration of dopamine in target areas. Although the exact mechanisms of pacemaking are still unclear, there is evidence that differences exist between pacemaking of DA neurons located in the substantia nigra pars compacta (SNc) and of those located in the ventral tegmental area (VTA), with the former relying more on Ca^{2+} channels and the latter on Na^+ channels (Puopolo et al., 2007; Khaliq and Bean, 2010). In addition, it has been suggested that SNc DA neurons, many of which are known to degenerate in Parkinson's disease, have a larger amount of L-type Ca^{2+} channels, than neighboring VTA DA neurons, which are spared in this disease (Surmeier, 2007). This might lead to a chronic Ca^{2+} overload in SNc DA neurons and induce a metabolic stress (Guzman et al., 2010). It is very important to test this hypothesis thoroughly because these L-type channels might be targeted pharmacologically, providing a potential neuroprotective strategy for these patients. Indeed, isradipine, a dihydropyridine calcium channel blocker, has been shown to be neuroprotective for SNc DA neurons in animal models of Parkinson's disease and is currently tested in a large clinical trial (Parkinson Study Group, 2013). Although it has been suggested that a higher L-type Ca^{2+} channel density could be causally related to the higher sensitivity to degeneration in Parkinson's disease, no study has directly compared the density of these currents in SNc and VTA DA neurons. Here, we have precisely measured the amplitude of somatic Ca^{2+} currents in both subsets of DA neurons using nucleated patch recordings in rat brain slices. We found that both the amplitude of the L-type Ca^{2+} current and its contribution to the total somatic Ca^{2+} current are higher in SNc DA neurons. On the contrary, the N-type current is more prominent in VTA DA neurons. We also compared the amplitude of the charge transfer through Ca^{2+} channels during physiological activity using the action potential and burst clamp method. As expected, we observed a larger charge transfer through L-type Ca^{2+} channels in SNc DA neurons.

Materials and Methods

Slice preparation. Midbrain slices used for patch-clamp recordings were obtained from Wistar rats of either sex between postnatal days 15 and 20. A previous study found that DA neurons have reached their mature electrophysiological phenotype at that age (Dufour et al., 2014a). Animals were killed by decapitation. The brain was quickly removed and placed in a chamber where it was submerged in an oxygenated ice-cold physiological saline solution (ACSF) containing the following (in mM): 125 NaCl, 2.5 KCl, 1 $MgCl_2$, 2 $CaCl_2$, 25 glucose, 1.25 NaH_2PO_4, 25 $NaHCO_3$, pH 7.4 (95% O_2 5% CO_2 and 310 mosm/L). Coronal 300-μm-thick slices were cut using a vibrating blade microtome (DTK-1000, Dosaka). Brain slices were incubated at 34°C for 30–60 min and thereafter stored at room temperature.

Electrophysiological recordings. For patch-clamp recordings, slices were placed into a recording chamber and continuously superfused with warm ACSF (30°). Neurons were visualized using a BX51WI Olympus microscope equipped with a CCD camera (ICD-42B, Ikegami). Patch-clamp recordings were obtained using low-resistance patch electrodes (3–5 MΩ) that were pulled from filamented borosilicate glass tubing (2.0 mm outer diameter, 0.42 mm wall thickness; Hilgenberg) with a PC-10 puller (Narishige). DA neurons were first targeted by their location within the SNc or the VTA. They were then identified in whole-cell mode based on various electrophysiological characteristics, including slow pacemaking (<5 Hz), action potential duration (width at half-amplitude >1.35 ms), and the presence of a robust hyperpolarization activated inward current (I_h) (Yung et al., 1991; Richards et al., 1997) (Fig. 1*A–D*). In addition, a subset of neurons was tested for the presence of D2 autoreceptors by quantifying the amplitude of the hyperpolarization induced by 100 μM dopamine (Fig. 1*E*). The sum of these criteria unambiguously identifies recorded neurons in the SNc and VTA as DA. However, in the VTA, only a subset of DA neurons, mostly meso-accumbens ones, satisfy these criteria (Lammel et al., 2008). Therefore, our conclusions are restricted to these neurons. Localization of DA neurons from which nucleated patches were extracted was achieved as follows: a picture of the localization of the pipette above the slice was taken at the end of each experiment and compared with the Paxinos and Watson atlas. Care was taken to avoid recordings in the area, which is at the junction between SNc and VTA. Localization of a subset of neurons from which nucleated patches were extracted is shown in Figure 1*F*. Signals were digitized with a Digidata 1440A interface and amplified with a Multiclamp 700B amplifier (Molecular Devices). Nucleated outside-out patches were extracted from the soma of DA neurons. For this purpose, negative pressure (170–190 mbar) was applied during the withdrawal of the patch pipette. Using a smooth retraction, we could obtain large patches of membrane surrounding the nucleus of the neuron. Following the extraction of the patch, the pressure was reduced to −50 mbar for the duration of the experiment. Data were sampled at 50 kHz and filtered at 10 kHz. Some traces in the figures were filtered digitally (Gaussian characteristics, 2 kHz). Specific protocols are described in detail in Results. Currents displayed in the figures were obtained after leak subtraction using a classical P/4 protocol.

For nonstationary fluctuation analysis (NSFA) (Sigworth, 1980), 15 to 38 current responses evoked by 20 ms depolarizing pulses from −100 to 10 mV were averaged, and the variance around the mean was calculated. To minimize errors caused by the run-down, ensemble variance versus time was measured as the average of variances from groups of 3 nonoverlapping traces (Engel and Jonas, 2005). The relationship between the mean current amplitude (I) and the variance (σ^2) was fitted with the equation $\sigma^2 = iI - I^2/N$, where i is the single-channel current amplitude and N is the estimate of the number of channels open at the peak of the current. The peak open probability (P_o, peak), corresponding to the fraction of available ion channels open at the time of the peak current (Ipeak) was calculated according to the following equation P_o, peak = Ipeak/(iN). The single-channel (unitary) conductance (γ) was extracted using this equation: $\gamma = I/(V_m - E_{rev})$, where V_m is the membrane potential (V_m) and E_{rev} the reversal potential, which was determined experimentally.

For nucleated patch recordings, the internal solution contained the following (in mM): 125 K-gluconate, 20 KCl, 10 HEPES, 4 Mg-ATP, 0.3 NaGTP, 10 Na_2-phosphocreatine, and 0.5 EGTA, pH 7.2 (302 mosm/L). For the action potential clamp experiments (which were performed in whole-cell mode), the internal solution contained the following (in mM): 120 $CsMeSO_4$, 20 CsCl, 10 HEPES, 2 $MgCl_2$, 2 Na_2ATP, 0.5 NaGTP, 5 Na_2-phosphocreatine, and 0.1 EGTA, pH 7.2 (302 mosm/L).

Slices were initially superfused with a control physiological saline solution (see composition above). When in the nucleated patch configuration, the solution was switched to the following (in mM): 110 NaCl, 2.5 KCl, 1 $MgCl_2$, 10 HEPES, 20 $BaCl_2$, 25 glucose, 3 4-AP, 20 TEA, 0.001 TTX, pH 7.4 (310 mosm/L) (adapted from Almog and Korngreen, 2009).

The following drugs were applied during pharmacological experiments (concentrations were chosen for maximal block of the target without losing specificity; a nonspecific effect on A-type currents has been reported for SNX-482 (Kimm and Bean, 2014), but this did not interfere with our experiments because these currents were blocked by 4-AP: nifedipine (5 μM), ω-conotoxin-GVIA (500 nM), ω-agatoxin (1 μM), SNX-482 (100 nM), and TTA-P2 (3,5-dichloro-N-[1-(2,2-dimethyl-tetrahydro-pyran-4-ylmethyl)-4-fluoro-piperidin-4-ylmethyl]-benzamide) (3 μM), which block L-, N-, P/Q-, R-, and T-type Ca^{2+} channels, respectively. The sources of the com-

pounds were as follows: ω-agatoxin and ω-conotoxin-GVIA were purchased from Bachem, nifedipine from Sigma, and SNX from Peptides International). TTA-P2 was generously provided by Merck.

Extracellular experiments were performed on adult male Wistar rat slices (6–8 weeks old) as previously described (Scuvee-Moreau et al., 2002). DA neurons were characterized by spontaneous and regular action potential firing (variation of <10% over a 5 min period), low firing frequencies (0.5–5.0 Hz), long action potential durations (>2 ms), and a strong inhibition of firing during application of the D2 agonist BHT920 (50 nM). This concentration of BHT920 inhibited the firing of neurons by 97.5 ± 2.6% in the VTA and 97.3 ± 2.0% in the SNc. When examining the effect of apamin and nifedipine, we isolated DA neurons pharmacologically by superfusing 10 μM CNQX, 10 μM SR95531, 1 μM MK801, 1 μM sulpiride, and 1 μM CGP55845, which block AMPA/kainate, $GABA_A$, NMDA, D2/D3, and $GABA_B$ receptors, respectively, both before and during application of the channel blockers. The source of the drugs not mentioned above was as follows: CGP55845, MK801, CNQX, and SR95531 were obtained from Tocris Bioscience. Apamin and sulpiride were purchased from Sigma. BHT920 was a gift from Boehringer Ingelheim. To quantify firing regularity, we measured the coefficient of variation (CV) of interspike intervals (ISIs), which was defined as follows: CV = SD_{ISI}/mean ISI. The CV was measured in the control period during the minute preceding superfusion of apamin, and during the last minute of a 10 min superfusion of apamin alone and of apamin + nifedipine.

Immunocytochemistry. Rats were deeply anesthetized with an injection of a mixture of ketamine and xylazine (80 and 10 mg/kg, respectively) before undergoing a thoracotomy. A cold 4°C PFA (4%) solution was then perfused intracardially for 15 min. Brains were collected, postfixed with 4% PFA, and cut into 30-μm-thick coronal sections using a cryostat. Immunolabeling was performed as described previously (Wolfart et al., 2001). First, slices were incubated in a blocking solution for 30 min at room temperature. Thereafter, three 10 min washes in PBS (0.01 M) were performed on an orbital shaker. Sections were then incubated in a solution containing two primary antibodies: a mouse TH antibody (Immunostar, reference 22941, 1/10000) and either a $Ca_v1.2$ or a $Ca_v1.3$ antibody from rabbit (Alomone Labs, references ACC-003 and ACC-005, 1/50 and 1/100, respectively) for 24 h at room temperature on an orbital shaker. Additional experiments performed with other antibodies against Ca^{2+} channel main subunits (Neuromab catalog #75-257 and #75-113 for $Ca_v1.2$ and $Ca_v1.3$, respectively, as well as an appropriate secondary antibody) yielded similar results (data not shown). Sections were subsequently washed three times for 10 min in PBS and incubated for 3 h with appropriate secondary antibodies: a goat anti-mouse IgG coupled to AlexaFluor-568 (ThermoFisher, 1/500) and a donkey anti-rabbit IgG coupled to fluorescein (Jackson ImmunoResearch Laboratories, 1/1000) at room temperature and in the dark. Finally, after three 10 min washes in PBS and 5 min incubation in Hoechst (Invitrogen, 1/5000), slices were mounted on slides, left to dry (in the dark at room temperature), and coverslipped with Fluorosave (Dako Denmark) mounting medium. All immunolabelings were viewed on a Leica SP5 confocal microscope (Leica Microsystems). Control experiments (incubation of either the primary or the secondary antibody alone, preincubation of the primary antibody with a blocking peptide) yielded no staining.

Data acquisition, analysis, and statistics. To exclude the influence of small variations in the size of the nucleated patches, voltage-clamp results were expressed as current density (i.e., the current amplitude was divided by the capacitance of the patch). Nucleated patch capacitances ranged

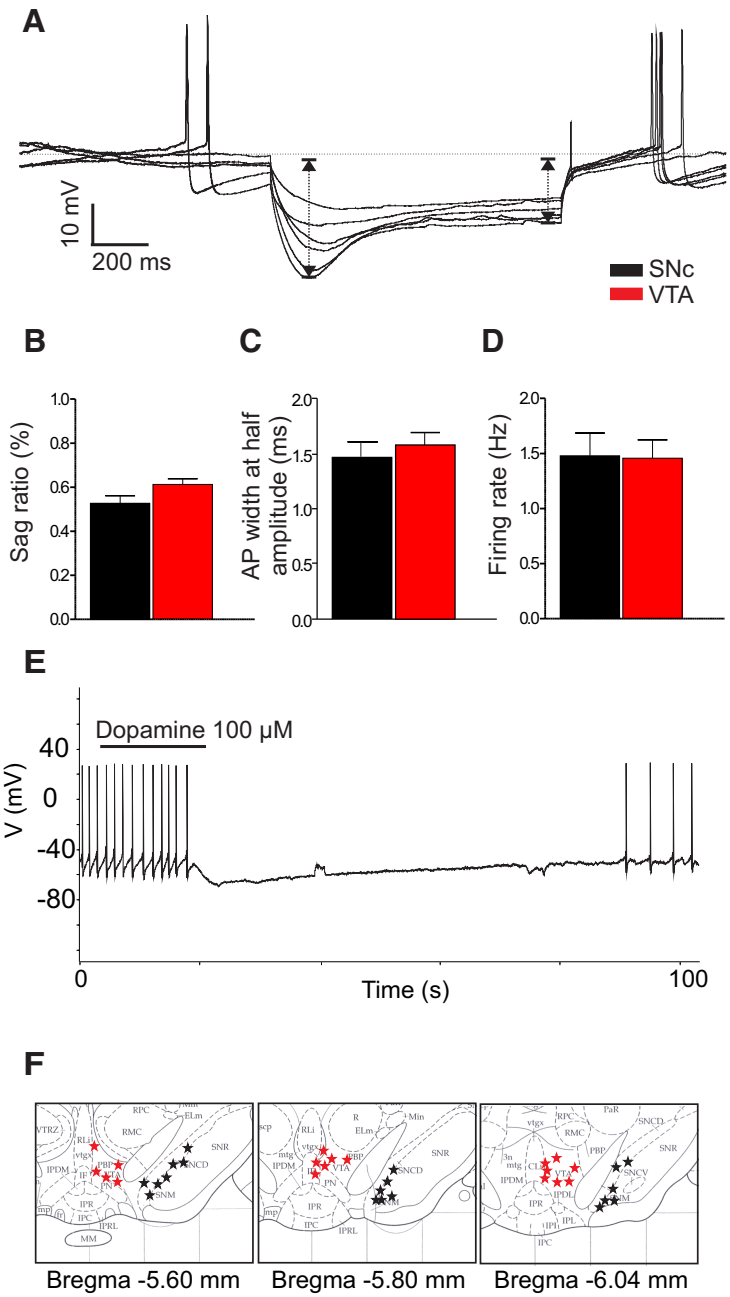

Figure 1. Functional characterization of recorded neurons in the whole-cell mode. In all figures: black columns represent dopaminergic neurons located in the SNc and red columns represent dopaminergic neurons located in the VTA. ***A***, Voltage traces evoked by a series of 1 s hyperpolarizing current pulses (from −40 pA to −140 pA, with an increment of −20 pA). This recording was from an SNc neuron. Arrows indicate the points where the ΔVs were measured to calculate the sag ratio (which was defined as the ΔV at the end of the pulse divided by the ΔV at the peak of the voltage deflection). Values of sag ratios measured in neurons from the two areas (***B***, $n = 16$; ***C***, $n = 29$; ***D***, $n = 20$) show the width of the action potential at half-amplitude and the firing frequency, respectively. ***E***, Typical example of the hyperpolarizing effect of 100 μM dopamine in a VTA DA neuron. ***F***, Localization of neurons recorded in the two areas.

from 1.5 to 2.5 pF and were similar in SNc and VTA DA neurons (1.730 ± 0.083 and 1.707 ± 0.079 pF, respectively, $n = 39$ and 43, respectively; $p = 0.82$). NSFA was performed with Mathematica 9 (Wolfram Research), as previously described (Engel and Jonas, 2005). The activation and inactivation curves were fitted using Mathematica to a Boltzmann equation as follows:

$$f = \frac{P\,(V - E_{rev})}{1 + e^{\frac{-V + Vhalf}{K}}}$$

where K is the slope factor, Vhalf is the voltage of half-activation, and P is an amplitude factor.

All numerical data were analyzed using Prism (Graphpad Software) and were expressed as mean ± SEM. Because of non-normality of most datasets, nonparametric tests were used in most cases except where indicated. Differences were considered significant at $p < 0.05$. The data reported in Figure 3 were analyzed by comparing the percentage of total charge contributed by a given Ca^{2+} current subtype in the SNc and VTA. Using Mann–Whitney tests, we compared the relative contribution of a given current subtype to the total current in the two areas. This was found to be the most appropriate statistical method because of the nature of the samples (values for all Ca^{2+} current subtypes could not be obtained in a given patch, precluding the use of a global test such as a Kruskal–Wallis test).

Results

Somatic L-type calcium currents in SNc and VTA DA neurons

The first question we addressed was whether the maximal somatic L-type Ca^{2+} current density differs in SNc and VTA DA neurons. We used Ba^{2+} (20 mM) as charge carrier to reduce the contamination by K^+ currents and maximize the amplitude of the Ca^{2+} current (Almog and Korngreen, 2009). As in previous reports (Lorenzon and Foehring, 1995), preliminary experiments showed that Ba^{2+} currents exhibited similar voltage dependence to those obtained with Ca^{2+}. Reliable Ba^{2+} currents were obtained in nucleated patches after the application of K^+ and Na^+ channel blockers. To isolate the L-type Ca^{2+} current component, we applied the specific L-type blocker nifedipine (5 μM) and subtracted traces after its application from control traces (Fig. 2*A*). In this first protocol, we used a holding potential of −60 mV, with a stimulation frequency of 1 Hz, to evaluate the amplitude of current, which was available from the approximate potential reached in the middle of the ISI. To exclude the influence of small variations in the size of the nucleated patches, voltage-clamp results were expressed as current density (i.e., the current amplitude divided by the capacitance; see Materials and Methods). SNc DA neurons exhibited a significantly larger L-type current than their VTA counterparts with a maximal amplitude at 10 mV of 17.8 ± 1.6 pA/pF ($n = 10$) in SNc DA neurons and 9.1 ± 1.8 pA/pF in VTA DA neurons ($n = 9$) ($p = 0.002$) (Fig. 2*B*,*C*). This difference was specific because the peak amplitudes of fast Na^+ currents recorded before the application of TTX (44.1 ± 8.5 and 50.6 ± 6.4 pA/pF, $n = 10$ in each region, respectively, $p = 0.24$) and K^+ currents recorded before applying K^+ channel blockers (peak: 209.4 ± 45.7 and 217.8 ± 50.9 pA/pF, $n = 10$ in each region, respectively, $p = 0.84$) were similar in the somata of the two types of neurons.

Relative contribution of various Ca^{2+} channel subtypes in SNc and VTA DA neurons

In the above experiments, the maximal total Ca^{2+} current was found to be similar in both types of DA neurons (19.7 ± 3.8 and 16.9 ± 3.3 pA/pF, $n = 10$ in each region, respectively, $p = 0.79$; Fig. 2*D*), suggesting that other Ca^{2+} currents might be more prominent in VTA DA neurons. To investigate this in detail, we performed a second series of experiments using a different holding potential (−100 mV instead of −60 mV). This was necessary to evaluate the availability of all Ca^{2+} channels, including low voltage-activated T-type channels. Again, the maximal total Ca^{2+} current amplitude in both areas was similar (peak current values were −76.1 ± 10.1 and −75.6 ± 16.9 pA/pF, in the SNc and VTA, respectively), but a difference in the extent of inactivation was clearly apparent (Fig. 3*A*). To take into account these two parameters (maximal amplitude and extent of inactivation), we calculated the charge transfer through the different types of channels in the two areas. Figure 3*A* shows the total Ca^{2+} current as well as the various Ca^{2+} current subtypes when isolated pharmacologically. The total charge transfer through Ca^{2+} channels was larger in the SNc than in the VTA in this protocol (Fig. 3*B*; $p = 0.03$). This was largely explained by the fact that the L-type current of SNc DA neurons was larger and inactivated to a lesser extent than the equivalent current recorded in VTA DA neurons. On the other hand, the relative amplitude of the N-type component was larger in VTA DA neurons. The percentage of the total charge transfer through the different channel subtypes is displayed in Figure 3*C*. This histogram shows an inverted relative contribution of the L- and the N-type calcium channels in the two regions, with a calcium entry relying more on L-type (42.3 ± 5.1%), and less so on N-type (24.9 ± 3.2%) channels in SNc DA neurons. On the contrary, there was a larger relative charge transfer through N-type channels (37.4 ± 3.8%) than through L-type channels (18.4 ± 2.2%) in VTA DA neurons ($p = 0.0004$ for the L-type contribution and $p = 0.031$ for the N-type contribution). Charge transfer through T-, R-, and P/Q-type channels was smaller and similar between both types of DA neurons.

Differences in L-type channel density and unitary current in SNc and VTA DA neurons

We next tested the hypothesis that differences at the single-channel level may underlie the differences found in the macroscopic characteristics of L-type currents, using NSFA (Sigworth, 1980) (see Materials and Methods). In this experiment, blockers of N, P/Q, R, and T channels were added to the solution to isolate the L-type component. We selected for these experiments nucleated patches, which exhibited no or little rundown during 30 consecutive steps (lasting 20 ms) from −100 to 10 mV with a stimulation frequency of 1 Hz (Fig. 4*A*, top). Filtering of individual sweeps was performed with a digital Gaussian filter at 2 kHz and current variance (σ^2) calculated from the difference between 30 consecutive sweeps. The curve of the variance versus the current could be fitted with a parabolic function (see Materials and Methods; Fig. 4*B*) and gave an estimated number of channels that was much larger in the SNc than in the VTA (502 ± 74 vs 160 ± 45 per patch; $n = 6$ for both regions; $p = 0.002$). However, somewhat surprisingly, the single-channel current was larger in the latter area: 0.83 ± 0.10 compared with 0.50 ± 0.03 pA in the SNc ($p = 0.041$). The open probability (P_0) was similar in the two areas (Fig. 4*C*–*E*). Together, these results demonstrate a higher density of L-type channels in the SNc and a differential single-channel conductance in the two areas.

Distribution pattern of $Ca_v1.3$ and $Ca_v1.2$ in SNc and VTA DA neurons

Globally, the electrophysiological data suggest that the molecular buildup of L channels (Buraei and Yang, 2013) may be different in the two areas. To start addressing this issue, we performed immunocytochemistry experiments. We first hypothesized that

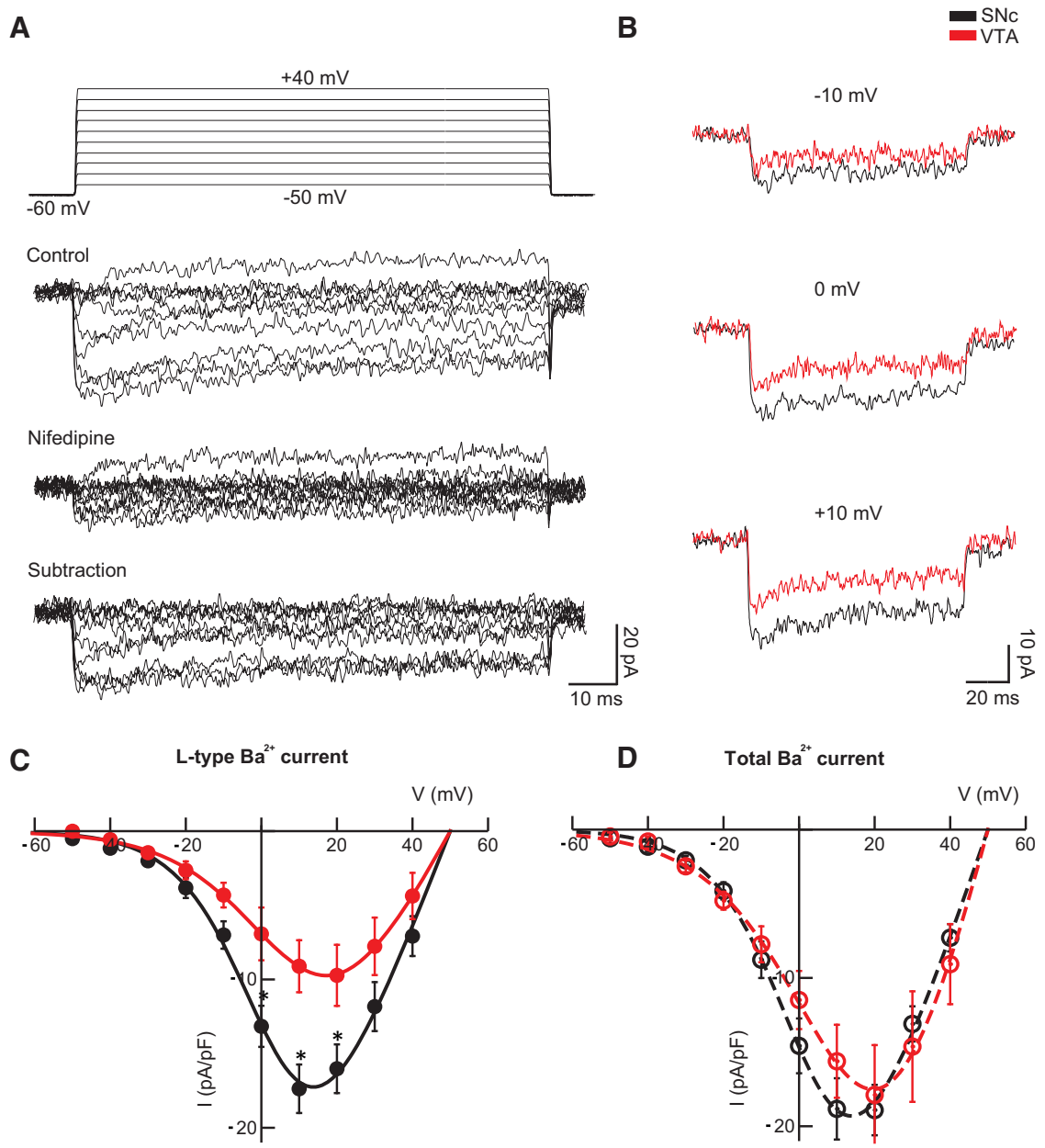

Figure 2. Somatic L-type Ca^{2+} currents are larger in SNc than in VTA DA neurons. ***A***, Methodology used to quantify L-type currents. Voltage protocol is shown. Top traces, Control conditions for an SNc DA neuron (using 20 mM Ba^{2+} as well as Na^+ and K^+ channel blockers; see Materials and Methods). Middle traces, In the presence of 5 μM nifedipine. Bottom traces, Subtractive traces showing the isolated L-type component. ***B***, Individual traces of isolated L-type currents in SNc and VTA DA neurons. Holding potential was −60 mV, and 150 ms pulses were made to the indicated voltages. ***C***, Current to voltage (I–V) relation of the L-type current in SNc (black, $n = 10$) and VTA (red, $n = 9$) DA neurons. Data were fitted with a Boltzmann function (see Materials and Methods). Currents were normalized to the capacitance of the patch. ***D***, Current to voltage (I–V) relation of the total Ba^{2+} current ($n = 10$). *$p < 0.05$.

differences could exist in the two areas in terms of the relative density of main subunits carrying these currents. Voltage-dependent Ca^{2+}channels are multimeric proteins in which the pore-forming α-subunit is the major determinant of gating and pharmacology. In the brain, two different α-subunits can be found: $Ca_v1.3$ and $Ca_v1.2$ (Chan et al., 2007). Because of their opening at more depolarized potentials, the latter are less susceptible to play a role in the pacemaking. On the contrary, channels composed of the $Ca_v1.3$ α subunit open at more hyperpolarized potentials, making them more suitable candidates to support pacemaking in SNc DA neurons (Koschak et al., 2001; Xu and Lipscombe, 2001; Olson et al., 2005; Chan et al., 2007; Dragicevic et al., 2014). It is generally believed that most α subunits of L-type channels are of the Ca_v 1.3 subtype in these neurons (Chan et al., 2007; Dufour et al., 2014b), although direct quantitative evidence is lacking. We thus investigated the expression of somatodendritic $Ca_v1.2$ and $Ca_v1.3$ in both SNc and VTA DA neurons in P15-P20 Wistar rats (Fig. 5). We observed a colabeling of $Ca_v1.3$ and TH in the soma as well as in the proximal dendrites of SNc and VTA DA neurons, whereas little or no $Ca_v1.2$ labeling was found in the soma of these neurons. Similar results were obtained with two different antibodies (see Materials and Methods). These results are consistent with those observed by Dufour et al. (2014b). The L-type calcium currents recorded from the soma of SNc and VTA DA neurons thus appear to be mainly mediated by

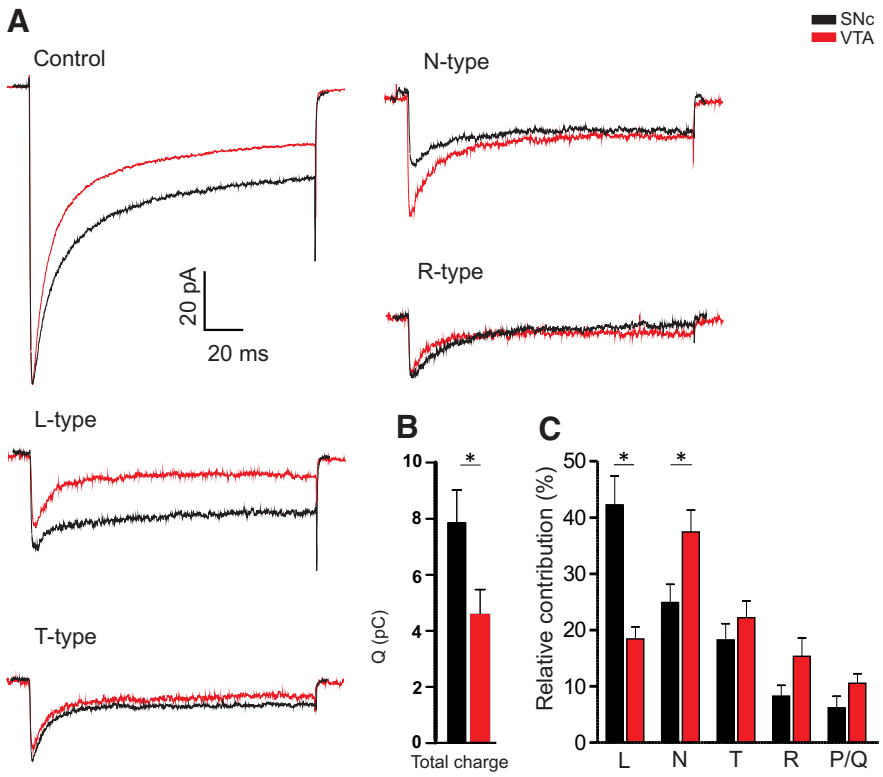

Figure 3. Relative contribution of individual Ca^{2+} current subtypes to the total charge transfer through Ca^{2+} channels is different in the SNc and VTA. ***A***, Currents evoked by a 150 ms step depolarization to 10 mV from a holding potential of −100 mV are shown before (control) and after application of Ca^{2+} channel blockers. The L, N, T, R, and P/Q currents were obtained by subtraction. ***B***, Total charge through all Ca^{2+} channels in the two areas. ***C***, The contribution of various Ca^{2+} current subtypes to the total charge transfer evoked by a pulse to 10 mV in SNc and VTA DA neurons. The contribution of each subtype is displayed in the histograms as a percentage of the total charge transfer. For methodological reasons, the sum of the contributions of all the channel subtypes was slightly >100%, and the individual contributions were subsequently normalized to yield a total of 100%. *$p < 0.05$.

$Ca_v1.3$ channels. Because immunocytochemistry is not quantitative, it was not possible from these experiments to evaluate a possible difference in channel density between the two areas. This result does not explain the functional differences that we found between SNc and VTA. Two alternative explanations for these differences are a differential expression of accessory (β) subunits or differential splicing of $Ca_v1.3$ subunits. These two phenomena have been shown to strongly influence inactivation (Bock et al., 2011).

Kinetic and inactivation properties of L-type Ca^{2+} channels in the two regions

Given the above mentioned NSFA results, we next tested whether specific biophysical properties of the L-type current could be different in DA neurons from the two regions. We first assessed activation, inactivation, and deactivation of this current in the two areas, given that differences in these properties could have a major effect on Ca^{2+} influx under physiological conditions. These experiments could only be done with Ba^{2+} as a charge carrier because currents evoked when using Ca^{2+} were clearly contaminated by unknown outward currents, as has also been observed in other neurons (see Almog and Korngreen, 2009). Therefore, we were unable to assess any inactivation or facilitation induced by Ca^{2+} in these cells (Soldatov et al., 1997; Kammermeier and Jones, 1998; Jenkins et al., 2010). Figure 6*A* shows the mean normalized activation curves of the Ba^{2+} current: no difference was found between SNc and VTA DA neurons. The $V_{1/2}$ values were 6.61 ± 2.79 and 8.21 ± 3.63 mV in the SNc and VTA, respectively ($p = 0.68$). Slope factors were also similar (10.55 ± 0.67 and 11.89 ± 1.67, $p = 0.96$; $n = 10$ for both measurements). The steady-state inactivation of the L current was also similar in both types of DA neurons ($V_{1/2}$ values were −23.00 ± 8.60 and −30.00 ± 4.32 mV in the SNc and VTA, respectively, whereas slope factors were −28.28 ± 2.78 and −28.74 ± 2.72, $p = 0.66$, $n = 7$ and $n = 5$, respectively; Fig. 6*B*). We finally measured the deactivation process by using a classical protocol (Fig. 6*C*) (Almog and Korngreen, 2009). A significant difference was found between the two populations of neurons (e.g., τ at −30 mV was 0.33 ± 0.05 ms in SNc DA neurons and 0.18 ± 0.03 ms in VTA DA neurons, $n = 7$ and $n = 5$, $p = 0.03$) (Fig. 6*D*).

Action potential clamp

We next evaluated one putative physiological correlate of the differences that we found in our voltage-clamp experiments (Fig. 7). For this purpose, "action potential clamp" and "burst clamp" experiments were performed using a physiological concentration of divalent cations (2 mM of either Ba^{2+} or Ca^{2+}). Divalent cation influx was also studied during bursting because this firing pattern has a major physiological significance in these neurons (Schultz, 2007); in addition, it might be more prevalent in the remaining neurons during the process of neurodegeneration in Parkinson's disease (Hollerman and Grace, 1990). Both influx through all Ca^{2+} channels and influx selectively through L-type channels were studied. For these experiments, 3 identical waveforms (dubbed −60, −50, and −40) recorded during *ex vivo* pacemaking and bursting (the latter being induced by coapplying 30 μM NMDA and 300 nM apamin and injecting −100 pA) were used as the command waveform in voltage-clamp mode. These waveforms were shifted by 10 mV because the exact value of membrane potentials during pacemaking is unknown. When examining values for action potential threshold reported in the literature, the −50 traces should be the closest to the real values, and we only report values for this protocol. Clear differences were again observed between DA neurons from the SNc and VTA. We performed our experiments first in 2 mM Ca^{2+} because two parameters of Ca^{2+} channel physiology (Ca^{2+}-dependent inactivation and facilitation) are only present in these conditions. These experiments could only be performed in the whole-cell mode because currents were too small in nucleated patches. We observed a larger total charge transfer (172.8 ± 28.6 vs 50.4 ± 12.7 pC, $n = 6$ in both groups, $p = 0.0159$) and a larger charge transfer through L-type channels (90.9 ± 24.5 vs 32.3 ± 10.3 pC, $p = 0.0152$) in SNc neurons than in VTA neurons in action potential clamp (Fig. 7*A*,*B*) as well as in burst clamp experiments (total charge: 284.3 ± 40.2 vs 116 ± 33.85 pC, $p = 0.028$; charge through L-type channels: 190.9 ± 23.7 vs 82.6 ± 32.1 pC, $p = 0.018$) (Fig. 7*C*,*D*). We noticed that the deactivation of the current seemed to be faster in the VTA (Fig. 7*A*,*C*, right

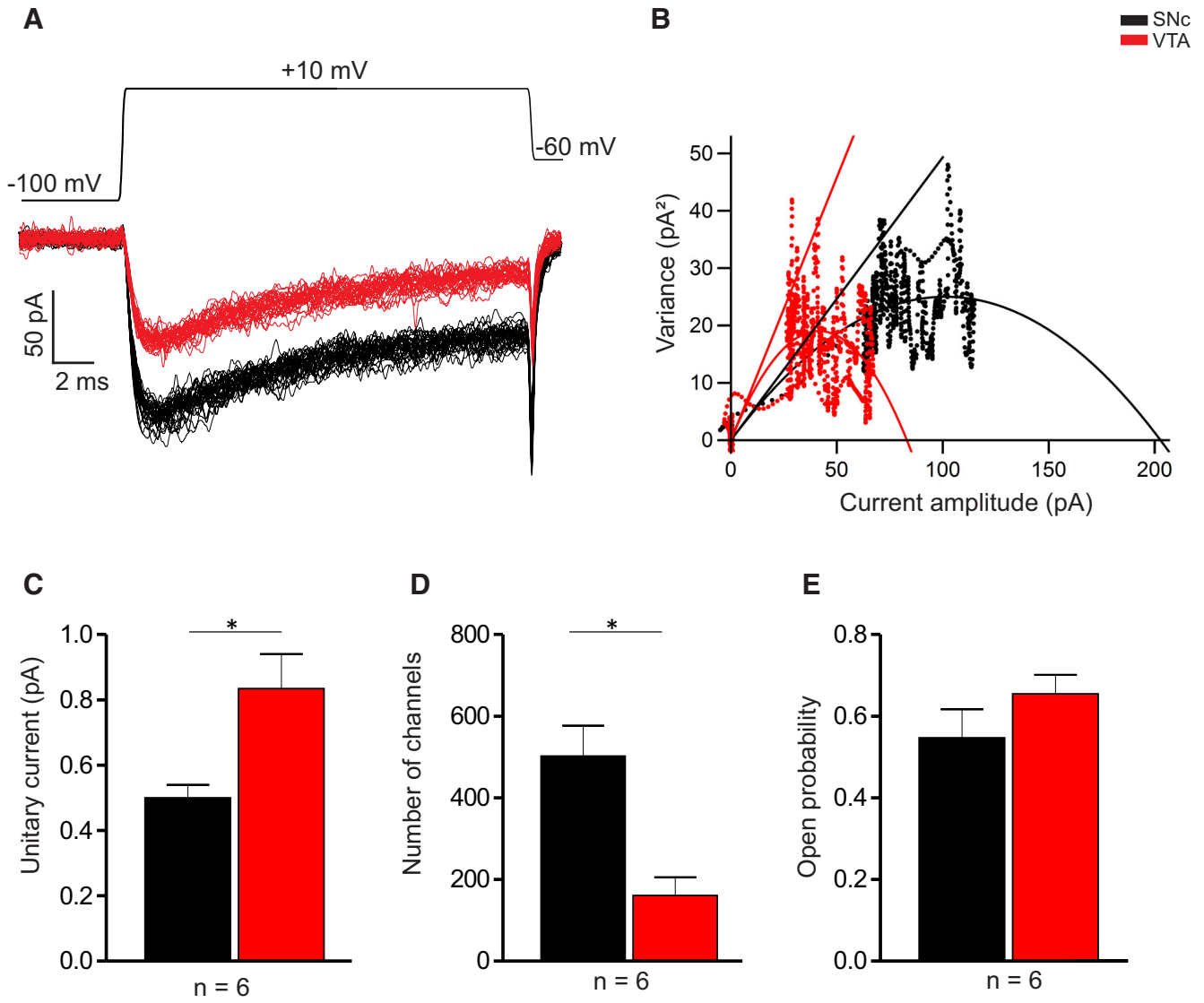

Figure 4. Nonstationary noise analysis of Ba^{2+} currents in nucleated patches. ***A***, Superimposed Ba^{2+} currents evoked by 30 depolarizing pulses from −100 to 10 mV in SNc and VTA DA neurons. L-type current was pharmacologically isolated by superfusing all blockers, except nifedipine. ***B***, Plot of variance against mean of current. Continuous lines indicate the fit according to $\sigma^2 = iI - I^2/N$. Data of two representative patches are shown. The baseline noise was subtracted. ***C–E***, Histograms showing the unitary current, the number of channels, and the open probability in neurons from both areas, respectively. *$p < 0.05$.

panels). This could be due to the difference in the deactivation process that we observed (Fig. 6*D*). Nevertheless, differences in the calcium inactivation/facilitation could also contribute to this phenomenon. To test this hypothesis, we performed the same experiments with 2 mM of Ba^{2+} instead of 2 mM Ca^{2+}. In this condition, there was no significant difference between charge transfer through L-type channels of SNc and VTA DA neurons, either in action potential (113.8 ± 24.5 vs 79.2 ± 18.78 pC, $p = 0.31$) or in burst clamp experiments (166.2 ± 15.6 vs 135.7 ± 40.6 pC, $p = 0.30$). Together, these data suggest that the higher calcium entry through L-type channels in SNc DA neurons is due to a larger amount of channels, less voltage-dependent inactivation, and possibly a differential sensitivity of the channels to intracellular Ca^{2+} compared with VTA DA neurons.

Impact on spontaneous firing patterns

To test another physiological correlate of L-type current density, we used extracellular recordings in slices from adult rats. It is known that the firing of SNc DA neurons becomes irregular in the slice preparation when their SK channels are completely blocked with 300 nM apamin and that this irregularity is counteracted by nifedipine (Shepard and Stump, 1999; Johnson and Wu, 2004; de Vrind et al., unpublished observation). This suggests that L-type channels promote firing irregularity in these neurons and that this "irregularity-promoting" effect is opposed by SK channels. We therefore asked whether the intensity of the "deregularization" would be different in the two areas. This was indeed the case. The increase in CV produced by apamin was 0.77 ± 0.16 and 0.37 ± 0.11 in the SNc (Fig. 8*A*,*B*) and VTA (Fig. 8*C*,*D*), respectively ($n = 14$ in both areas, $p = 0.02$). It was strongly reduced by 5 μM nifedipine in both areas. These results confirm the lower influence of L-type channels during block of SK channels in VTA DA neurons compared with their SNc counterparts.

Discussion

Globally, our results show that the density of L-type channels and their relative contribution to the total somatic Ca^{2+} current are

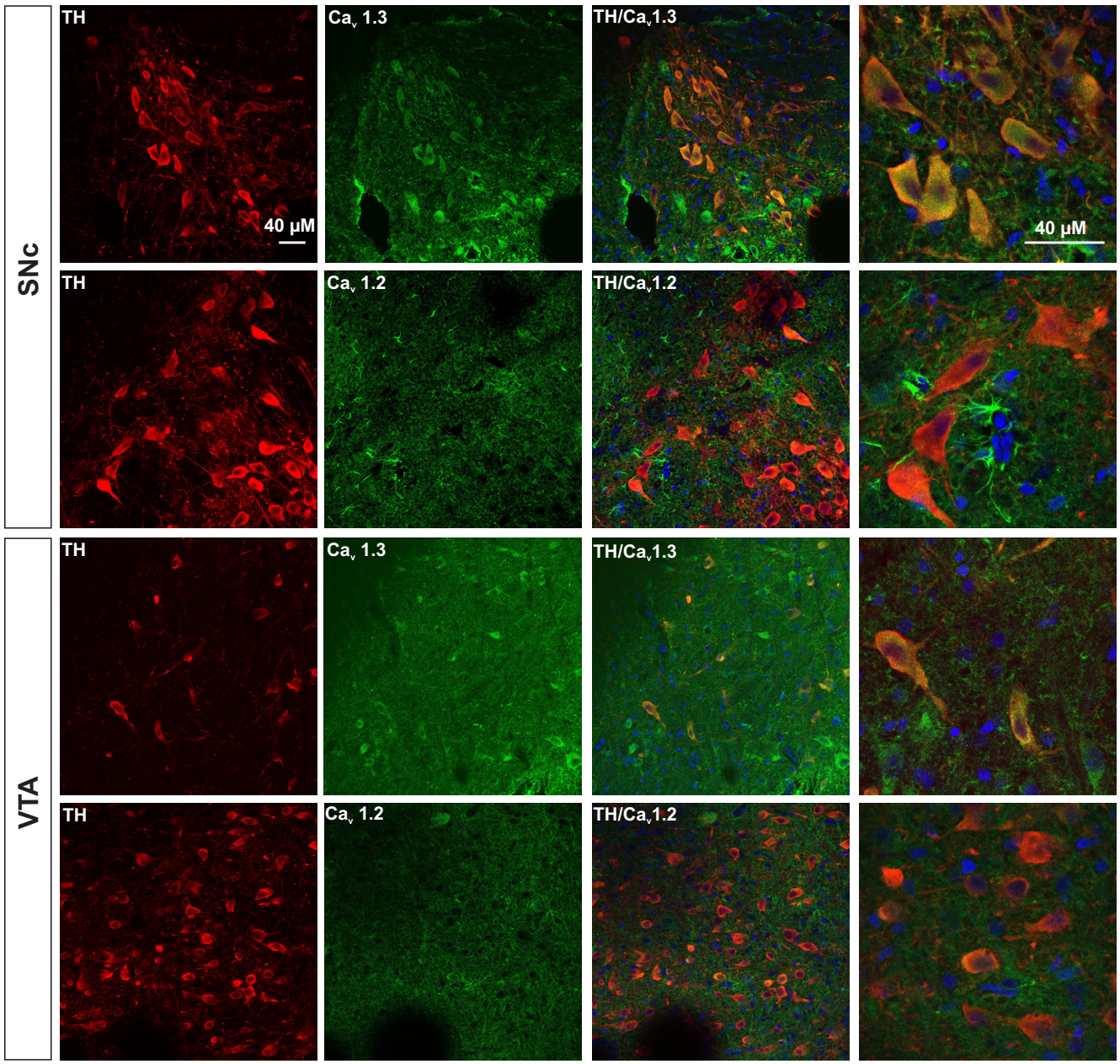

Figure 5. Ca$_v$1.3 immunoreactivity largely predominates both in SNc and VTA. Red represents TH labeling. Green represents Ca$_v$1.3 or Ca$_v$1.2. The third column represents the colabeling of TH, Ca$_v$ subunits, and nuclei (DAPI, blue). Original magnifications: left, middle, 40×; right, 120×. Colabeling of TH with Ca$_v$1.3 is obvious, whereas this is not the case for Ca$_v$1.2.

different in rat SNc and VTA neurons despite the fact that many macroscopic whole-cell parameters of these neurons (firing rate, action potential duration, hyperpolarizing effect of dopamine, I_h current) are almost indistinguishable (Fig. 1) (Lammel et al., 2008). Although a majority of our data deal with properties of the somatic area, these results strongly suggest that identical pacemaking can be obtained in these neurons with different Ca^{2+} channel densities, a proposal already made by Khaliq and Bean (2010), who suggested that the main current driving spontaneous pacemaking is a Ca^{2+} current in SNc DA neurons and a mixture of voltage-dependent and leak Na^+ currents in VTA DA neurons. The concept that variable combinations of ion channels can lead to similar firing properties has been amply demonstrated in invertebrate neurons (Goaillard et al., 2009). Our results suggest, but do not prove, that this notion could be valid as well in mammalian DA neurons. Our data do not exclude the possibility of other differences between these two groups of neurons, for example, in terms of densities of dendritic or axonal currents. Nor does it preclude the fact that SNc DA neurons may have heterogeneous electrical properties. Indeed, the existence of functionally distinct SNc DA neuron populations has been suggested by the work of others (Neuhoff et al., 2002; Evans and Khaliq, 2015). In addition, some of the parameters that we measured were also quite variable; for example, the percentage contribution of the L-type current to the total Ca^{2+} current in the SNc ranged from 16% to 81%. It will be interesting in future experiments to test whether this parameter correlates to other ones, such as the expression of calbindin or the projection area (Surmeier et al., 2010).

The results of our extracellular recordings demonstrate that differences in L-type channel density in the two areas have significant physiological consequences. Indeed, whereas complete block of SK channels by apamin markedly enhanced irregularity

in SNc neurons (as found repeatedly in previous studies, see references above), this was much less the case in VTA neurons. In addition, nifedipine suppressed the irregularity in both areas. Together, these results are consistent with the notion that, during complete blockade of SK channels, irregularity is promoted by L-type channels, and more so in SNc than in VTA DA neurons. Previous experiments show that these channels do not provide the Ca^{2+} that activates SK channels in these cells (for further discussion, see below). In addition, our extracellular experiments were performed in horizontal slices from adult rats, thus making it unlikely that the differences that we found between neurons from the two areas in nucleated patches are restricted to juvenile animals.

One slight internal inconsistency of our data pertains to the different outcome of experiments performed using 20 mM Ba^{2+} in nucleated patches and 2 mM Ba^{2+} in action potential clamp experiments in whole-cell mode. Thus, although somatic Ba^{2+} currents (measured using nucleated patches) were clearly larger in the SNc, the whole-cell charge transfer through L-type channels was not different in the two areas when 2 mM Ba^{2+} was used (although a trend was observed), whereas it was clearly different with 2 mM Ca^{2+} (Fig. 7). This inconsistency may be due to several factors: first, it is possible that the dendritic buildup of Ca^{2+} channels (which contributes to the current measured during action potential clamp, but not in the nucleated patch experiments) is different from the somatic one. Second, our nucleated patch experiments show that the maximal amount of L-type Ba^{2+} current, as tested using 20 mM Ba^{2+} is higher in the SNc, but it is possible that this amount is not recruited during "physiological" firing in 2 mM Ba^{2+} (except perhaps during the action potential, where the Ba^{2+} current is higher in the SNc than in the VTA in the action potential clamp experiments; data not shown). Indeed, in the voltage-clamp experiments using a holding potential of −60 mV, the current was larger in the SNc only at some test pulse potentials (Fig. 2*C*). Finally, it could be that Ca^{2+}-dependent modulation (inactivation or facilitation) (Kammermeier and Jones, 1998) of these channels is important as well and different in the two areas, a possibility that is realistic given their probably different molecular buildup (see below). For technical reasons, we were unable to test that hypothesis.

Our NSFA data suggest that, besides a differential density of L-type channels, midbrain DA neurons may express different types of Ca^{2+} channel subunits, although the exact nature of the difference remains unknown. From our immunocytochemistry data, it appears that the most abundant α_1 subunits in both areas are of the 1.3 subtype. However, because immunocytochemistry is not quantitative, we certainly cannot exclude the possibility of a differential ratio between the two subunits in the two areas. Further investigation on this issue (i.e., shRNA mediated down-regulation of main and accessory subunits in both areas using TH-Cre rats or transcriptomic analysis of microdissected neurons) may yield additional information. It is rather counterintuitive that the L-type single-channel conductance inferred from NSFA measurements was smaller in SNc neurons. However, this was more than compensated by a much larger number of these channels in this area. It is possible that, in addition to differential accessory subunits, these differences are also due to different microenvironments of the channels in the two areas. For example, there is indirect evidence that differences in palmitoylation of α subunits may impact single-channel conductance of L-type channels (Chien et al., 1996). Another possible difference between DA neurons from the two areas could be the amount of RNA editing of the subunits, a phenomenon that is known to affect Ca^{2+}-dependent inactivation (Huang et al., 2012; Bazzazi et al., 2013).

Globally, our results are congruent with the idea of a higher Ca^{2+} influx through L-type channels in SNc neurons compared with their VTA counterparts (Guzman et al., 2010). The current density difference is not very large, at least in the soma, but induces a clearly larger Ca^{2+} influx during physiological activity (our experiments do not allow to evaluate the relative involvement of somatic and dendritic channels to this influx). Our experiments were performed in wild-type rat slices (vs experiments in transgenic mice by Guzman et al., 2010; Khaliq and Bean, 2010), thus generalizing the concept of a higher Ca^{2+} influx through L-type channels in SNc DA neurons to more than one species. It would be important in the framework of this hypoth-

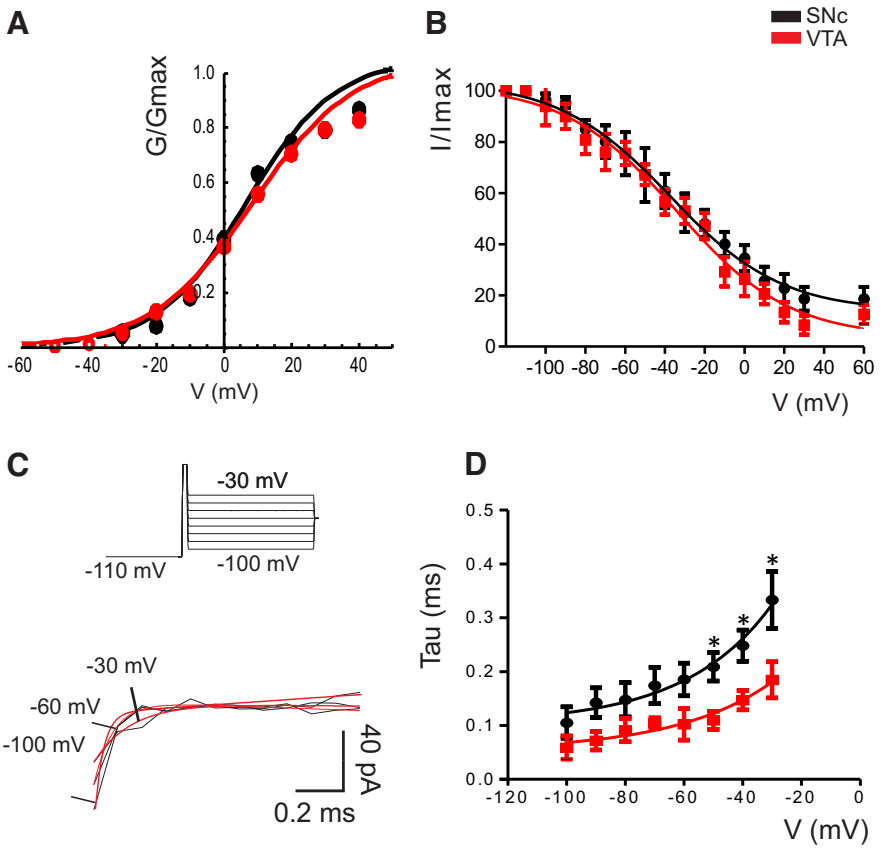

Figure 6. Some biophysical properties of L-type calcium channels are different in DA neurons from the two areas. ***A***, Activation curves. Peak Ba^{2+} permeability, normalized to the maximal value, is plotted as a function of voltage. Permeability values were obtained as described in Materials and Methods. Curves represent Boltzmann functions fitted to the data points. ***B***, Summary plot of L-type channel steady-state inactivation curves. Peak Ba^{2+} current amplitudes were normalized to the Ba^{2+} current obtained with the prepulse from −110 mV. Data points were fitted with Boltzmann functions. ***C***, Time courses of deactivation in an SNc DA neuron. Deactivation was measured as shown in the inset. ***D***, Summary plot of the time constant of deactivation. *$p < 0.05$.

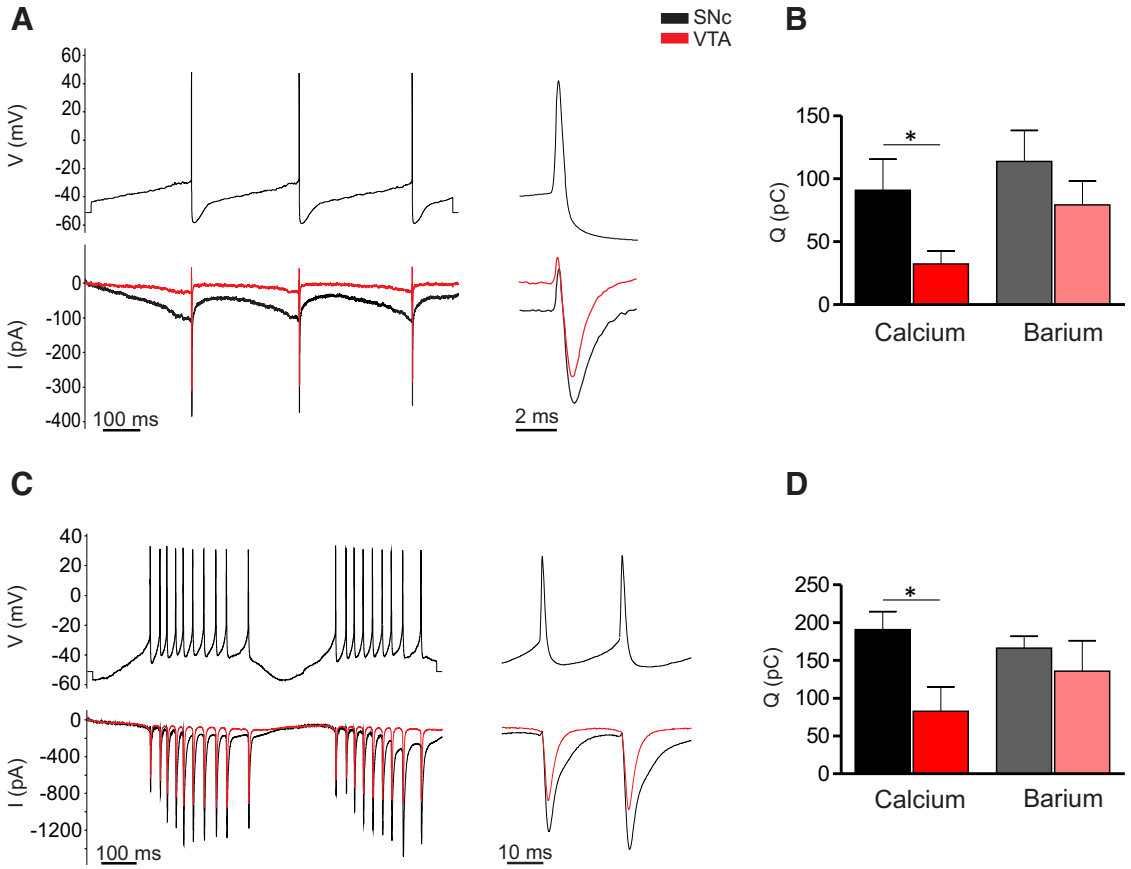

Figure 7. Charge transfer through L-type calcium channels evoked by action potential waveforms in the whole-cell configuration. ***A***, Pharmacologically isolated L-type calcium current evoked by a pacemaker waveform in SNc (black) and VTA (red) DA neurons. ***B***, Histogram representing the charge transfer through L-type channels in SNc and VTA DA neurons with either Ca^{2+} or Ba^{2+} as the charge carrier. ***C***, Pharmacologically isolated L-type calcium current evoked by a bursting waveform in SNc and VTA DA neurons. ***D***, Histogram showing the charge transfer through L-type channels in SNc and VTA DA neurons with either Ca^{2+} or Ba^{2+} as the charge carrier. $*p < 0.05$.

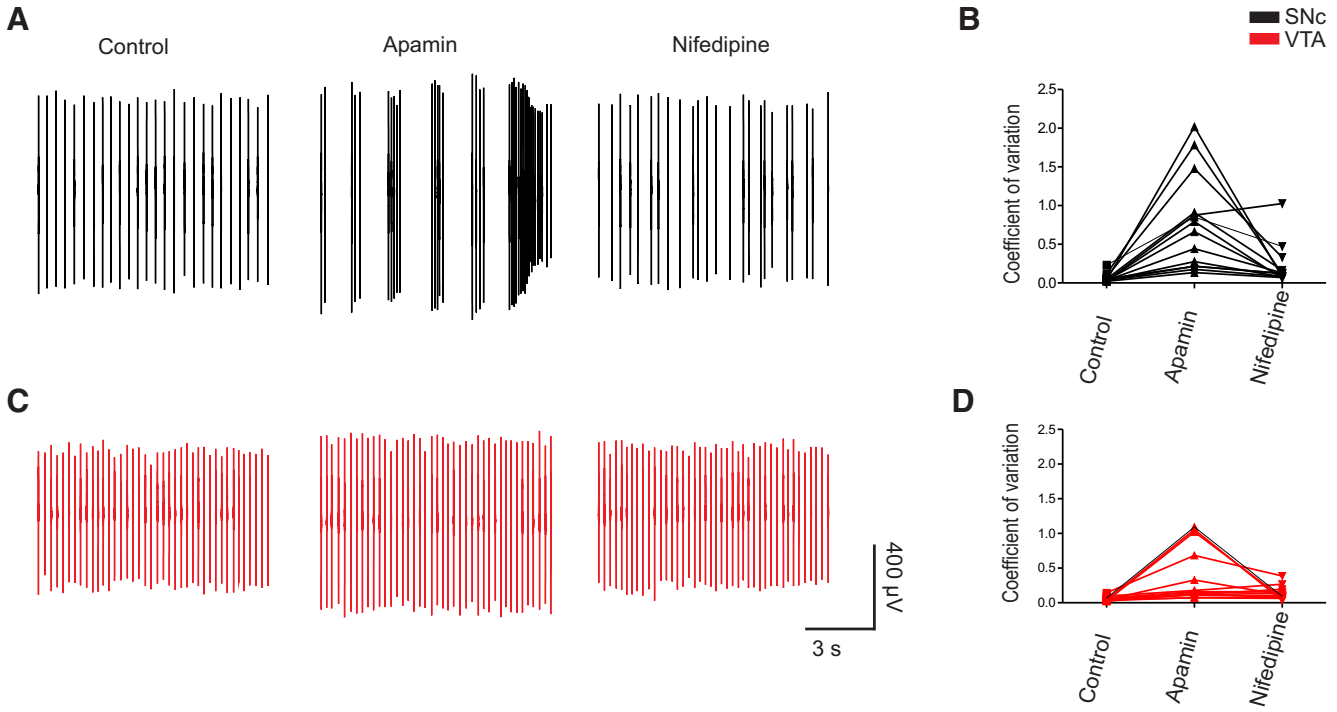

Figure 8. Apamin deregularizes DA neurons to a larger extent in SNc than in VTA DA neurons. ***A***, ***C***, Traces of extracellular recordings in one neuron of each area in control conditions and in the presence of apamin or nifedipine + apamin. ***B***, ***D***, Summary data on the CV of DA neurons in both areas.

esis to know whether the difference increases with age [note, however, that a recent study (Branch et al., 2014) reported results consistent with an opposite view, but it was performed only in SNc neurons and it measured only whole-cell currents] and/or is potentiated when DA neurons are chronically exposed to oxidizing conditions. In this respect, recent experiments on cardiomyocytes (which express $Ca_v1.2$) have shown that H_2O_2 potentiates L-type currents (Yang et al., 2013).

Why would Ca^{2+} entry through L-type channels be more toxic to DA neurons than Ca^{2+} entry through other sources? One possibility could be that L-type channels are open during a large part of the pacemaker cycle in these cells. However, in our action potential clamp experiments, charge transfer through these channels made up only approximately half of the charge transfer through all Ca^{2+} channels (the proportion being approximately two-thirds during bursting). A selective toxicity of L-type channels has been demonstrated in chromaffin cells (Cano-Abad et al., 2001), which also are slow pacemakers. It may be that L-type channels are closer to mitochondria than other membrane Ca^{2+} sources. What is clear is that these channels are not coupled to SK channels in DA neurons (the main source for activating these being T-type channels in neonatal mice and N-type channels in adult rats) (Wolfart et al., 2002; de Vrind et al., unpublished observations) and will therefore not indirectly activate "protective" K^+ channels.

The results of this study also allow to make progress toward a realistic model (or several models) of DA neuron physiology. We now have at hand a quantitative description of somatic voltage-dependent Na^+ (Seutin and Engel, 2010), Ca^{2+} (this study), and K^+ conductances (Gentet and Williams, 2007; Segev and Korngreen, 2007; Kimm et al., 2015). What is further needed is a quantification of somatic SK channel density. A precise knowledge of ion channel density in distal dendrites is not absolutely needed because it has been demonstrated that pacemaking in DA neurons is maintained in the absence of distal dendrites (Puopolo et al., 2005). One problematic issue will be the density of Na^+ channels in the axonal initial segment. Possibly, this unknown parameter could be approximated using the so-called "genetic algorithm" used by Almog and Korngreen (2014) to establish a realistic model of cortical layer 5 pyramidal neurons.

In conclusion, we show here that somatic Ca^{2+} channel populations are different in VTA and SNc DA neurons. This finding may have both physiological and pathophysiological implications.

References

Almog M, Korngreen A (2009) Characterization of voltage-gated Ca^{2+} conductances in layer 5 neocortical pyramidal neurons from rats. PLoS One 4:e4941. CrossRef

Almog M, Korngreen A (2014) A quantitative description of dendritic conductances and its application to dendritic excitation in layer 5 pyramidal neurons. J Neurosci 34:182–196. CrossRef Medline

Bazzazi H, Ben Johny M, Adams PJ, Soong TW, Yue DT (2013) Continuously tunable Ca^{2+} regulation of RNA-edited CaV1.3 channels. Cell Rep 5:367–377. CrossRef Medline

Bernard G, Shevell MI (2008) Channelopathies: a review. Pediatr Neurol 38:73–85. CrossRef Medline

Bock G, Gebhart M, Scharinger A, Jangsangthong W, Busquet P, Poggiani C, Sartori S, Mangoni ME, Sinnegger-Brauns MJ, Herzig S, Striessnig J, Koschak A (2011) Functional properties of a newly identified C-terminal splice variant of Cav1.3 L-type Ca^{2+} channels. J Biol Chem 286:42736–42748. CrossRef Medline

Branch SY, Sharma R, Beckstead MJ (2014) Aging decreases L-type calcium channel currents and pacemaker firing fidelity in substantia nigra dopamine neurons. J Neurosci 34:9310–9318. CrossRef Medline

Buraei Z, Yang J (2013) Structure and function of the β subunit of voltage-gated Ca^{2+} channels. Biochim Biophys Acta 1828:1530–1540. CrossRef Medline

Cameron DL, Wessendorf MW, Williams JT (1997) A subset of ventral tegmental area neurons is inhibited by dopamine, 5-hydroxytryptamine and opioids. Neuroscience 77:155–166. CrossRef Medline

Cano-Abad MF, Villarroya M, García AG, Gabilan NH, López MG (2001) Calcium entry through L-type calcium channels causes mitochondrial disruption and chromaffin cell death. J Biol Chem 276:39695–39704. CrossRef Medline

Chan CS, Guzman JN, Ilijic E, Mercer JN, Rick C, Tkatch T, Meredith GE, Surmeier DJ (2007) "Rejuvenation" protects neurons in mouse models of Parkinson's disease. Nature 447:1081–1086. CrossRef Medline

Chien AJ, Carr KM, Shirokov RE, Rios E, Hosey MM (1996) Identification of palmitoylation sites within the L-type calcium channel beta2a subunit and effects on channel function. J Biol Chem 271:26465–26468. CrossRef Medline

Chung CY, Seo H, Sonntag KC, Brooks A, Lin L, Isacson O (2005) Cell type-specific gene expression of midbrain dopaminergic neurons reveals molecules involved in their vulnerability and protection. Hum Mol Genet 14:1709–1725. CrossRef Medline

Dragicevic E, Poetschke C, Duda J, Schlaudraff F, Lammel S, Schiemann J, Fauler M, Hetzel A, Watanabe M, Lujan R, Malenka RC, Striessnig J, Liss B (2014) Cav1.3 channels control D2-autoreceptor responses via NCS-1 in substantia nigra dopamine neurons. Brain 137:2287–2302. CrossRef Medline

Dufour MA, Woodhouse A, Amendola J, Goaillard JM (2014a) Non-linear developmental trajectory of electrical phenotype in rat substantia nigra pars compacta dopaminergic neurons. Elife 2014:3. CrossRef Medline

Dufour MA, Woodhouse A, Goaillard JM (2014b) Somatodendritic ion channel expression in substantia nigra pars compacta dopaminergic neurons across postnatal development. J Neurosci Res 92:981–999. CrossRef Medline

Engel D, Jonas P (2005) Presynaptic action potential amplification by voltage-gated Na^+ channels in hippocampal mossy fiber boutons. Neuron 45:405–417. CrossRef Medline

Evans RC, Khaliq ZM (2015) T-type calcium channels control non-linear dendritic integration in a vulnerable subpopulation of substantia nigra dopamine neurons. Soc Neurosci Abstr 801.03.

Fields HL, Hjelmstad GO, Margolis EB, Nicola SM (2007) Ventral tegmental area neurons in learned appetitive behavior and positive reinforcement. Annu Rev Neurosci 30:289–316. CrossRef Medline

Gentet LJ, Williams SR (2007) Dopamine gates action potential backpropagation in midbrain dopaminergic neurons. J Neurosci 27:1892–1901. CrossRef Medline

Goaillard JM, Taylor AL, Schulz DJ, Marder E (2009) Functional consequences of animal-to-animal variation in circuit parameters. Nat Neurosci 12:1424–1430. CrossRef Medline

Grimm J, Mueller A, Hefti F, Rosenthal A (2004) Molecular basis for catecholaminergic neuron diversity. Proc Natl Acad Sci U‖S|A 101:13891–13896. CrossRef Medline

Guzman JN, Sanchez-Padilla J, Wokosin D, Kondapalli J, Ilijic E, Schumacker PT, Surmeier DJ (2010) Oxidant stress evoked by pacemaking in dopaminergic neurons is attenuated by DJ-1. Nature 468:696–700. CrossRef Medline

Häusser M, Stuart G, Racca C, Sakmann B (1995) Axonal initiation and active dendritic propagation of action potentials in substantia nigra neurons. Neuron 15:637–647. CrossRef Medline

Hollerman JR, Grace AA (1990) The effects of dopamine-depleting brain lesions on the electrophysiological activity of rat substantia nigra dopamine neurons. Brain Res 533:203–212. CrossRef Medline

Huang H, Tan BZ, Shen Y, Tao J, Jiang F, Sung YY, Ng CK, Raida M, Köhr G, Higuchi M, Fatemi-Shariatpanahi H, Harden B, Yue DT, Soong TW (2012) RNA editing of the IQ domain in Cav1.3 channels modulates their Ca^{2+}-dependent inactivation. Neuron 73:304–316. CrossRef Medline

Jenkins MA, Christel CJ, Jiao Y, Abiria S, Kim KY, Usachev YM, Obermair GJ, Colbran RJ, Lee A (2010) Ca^{2+}-dependent facilitation of Cav1.3 Ca^{2+} channels by densin and Ca^{2+}/calmodulin-dependent protein kinase II. J Neurosci 30:5125–5135. CrossRef Medline

Johnson SW, Wu YN (2004) Multiple mechanisms underlie burst firing in rat midbrain dopamine neurons in vitro. Brain Res 1019:293–296. CrossRef Medline

Kammermeier PJ, Jones SW (1998) Facilitation of L-type calcium current in thalamic neurons. J Neurophysiol 79:410–417. Medline

Khaliq ZM, Bean BP (2010) Pacemaking in dopaminergic ventral tegmental area neurons: depolarizing drive from background and voltage-dependent sodium conductances. J Neurosci 30:7401–7413. CrossRef Medline

Kimm T, Bean BP (2014) Inhibition of A-type potassium current by the peptide toxin SNX-482. J Neurosci 34:9182–9189. CrossRef Medline

Kimm T, Khaliq ZM, Bean BP (2015) Differential regulation of action potential shape and burst-frequency firing by BK and Kv2 channels in substantia nigra dopaminergic neurons. J Neurosci 35:16404–16417. CrossRef Medline

Koschak A, Reimer D, Huber I, Grabner M, Glossmann H, Engel J, Striessnig J (2001) 1D (Cav1.3) subunits can form L-type Ca^{2+} channels activating at negative voltages. J Biol Chem 276:22100–22106. CrossRef Medline

Lammel S, Hetzel A, Häckel O, Jones I, Liss B, Roeper J (2008) Unique properties of mesoprefrontal neurons within a dual mesocorticolimbic dopamine system. Neuron 57:760–773. CrossRef Medline

Liss B, Roeper J (2008) Individual dopamine midbrain neurons: functional diversity and flexibility in health and disease. Brain Res Rev 58:314–321. CrossRef Medline

Lorenzon NM, Foehring RC (1995) Characterization of pharmacologically identified voltage- gated calcium channel currents in acutely isolated rat neocortical neurons: II. Postnatal development. J Neurophysiol 73: 1443–1451. Medline

Magee JC (1999) Voltage-gated ion channels in dendrites. In: Dendrites (Stuart G, Spruston N, Hausser M, eds), pp 139–160. New York: Oxford University.

Margolis EB, Mitchell JM, Ishikawa J, Hjelmstad GO, Fields HL (2008) Midbrain dopamine neurons: projection target determines action potential duration and dopamine D2 receptor inhibition. J Neurosci 28:8908–8913. CrossRef Medline

Neuhoff H, Neu A, Liss B, Roeper J (2002) I(h) channels contribute to the different functional properties of identified dopaminergic subpopulations in the midbrain. J Neurosci 22:1290–1302. Medline

Nieoullon A (2002) Dopamine and the regulation of cognition and attention. Prog Neurobiol 67:53–83. CrossRef Medline

Olson PA, Tkatch T, Hernandez-Lopez S, Ulrich S, Ilijic E, Mugnaini E, Zhang H, Bezprozvanny I, Surmeier DJ (2005) G-protein-coupled receptor modulation of striatal CaV1.3 L-type Ca^{2+} channels is dependent on a shank-binding domain. J Neurosci 25:1050–1062. CrossRef Medline

Poulin JF, Zou J, Drouin-Ouellet J, Kim KY, Cicchetti F, Awatramani RB (2014) Defining midbrain dopaminergic neuron diversity by single-cell gene expression profiling. Cell Rep 9:930–943.

Puopolo M, Bean BP, Raviola E (2005) Spontaneous activity of isolated dopaminergic periglomerular cells of the main olfactory bulb. J Neurophysiol 94:3618–3627. CrossRef Medline

Puopolo M, Raviola E, Bean BP (2007) Roles of subthreshold calcium current and sodium current in spontaneous firing of mouse midbrain dopamine neurons. J Neurosci 27:645–656. CrossRef Medline

Richards CD, Shiroyama T, Kitai ST (1997) Electrophysiological and immunocytochemical characterization of GABA and dopamine neurons in the substantia nigra of the rat. Neuroscience 80:545–557. CrossRef Medline

Schultz W (2007) Multiple dopamine functions at different time courses. Annu Rev Neurosci 30:259–288. CrossRef Medline

Scuvee-Moreau J, Liegeois JF, Massotte L, Seutin V (2002) Methyl-laudanosine: a new pharmacological tool to investigate the function of small-conductance Ca(2+)-activated K(+) channels. J Pharmacol Exp Ther 302:1176–1183. CrossRef Medline

Segev D, Korngreen A (2007) Kinetics of two voltage-gated K^+ conductances in substantia nigra dopaminergic neurons. Brain Res 1173:27–35. CrossRef Medline

Seutin V, Engel D (2010) Differences in Na^+ conductance density and Na^+ channel functional properties between dopamine and GABA neurons of the rat substantia nigra. J Neurophysiol 103:3099–3114. CrossRef Medline

Shepard PD, Stump D (1999) Nifedipine blocks apamin-induced bursting activity in nigral dopamine-containing neurons. Brain Res 817:104–109. CrossRef Medline

Sigworth F (1980) The variance of sodium current fluctuations at the node of Ranvier J Physiol 307:97–129. CrossRef

Soldatov NM, Zühlke RD, Bouron A, Reuter H (1997) Molecular structures involved in L-type calcium channel inactivation. J Biol Chem 272:3560–3566. CrossRef Medline

Surmeier DJ (2007) Calcium, ageing, and neuronal vulnerability in Parkinson's disease. Lancet Neurol 6:933–938. CrossRef Medline

Surmeier DJ, Guzman JN, Sanchez-Padilla J (2010) Calcium, cellular aging, and selective neuronal vulnerability in Parkinson's disease. Cell Calcium 47:175–182. CrossRef Medline

Parkinson Study Group (2013) Phase II safety, tolerability, and dose selection study of isradipine as a potential disease-modifying intervention in early Parkinson's disease (STEADY-PD). Mov Disord 28:1823–1831. CrossRef Medline

Wise RA (2004) Dopamine, learning and motivation. Nat Rev Neurosci 5:483–494. CrossRef Medline

Wolfart J, Roeper J (2002) Selective coupling of T-type calcium channels to SK potassium channels prevents intrinsic bursting in dopaminergic midbrain neurons. J Neurosci 22:3404–3413. Medline

Wolfart J, Neuhoff H, Franz O, Roeper J (2001) Differential expression of the small-conductance, calcium-activated potassium channel SK3 is critical for pacemaker control in dopaminergic midbrain neurons. J Neurosci 21:3443–3456.

Xu W, Lipscombe D (2001) Neuronal Ca(V)1.3alpha(1) L-type channels activate at relatively hyperpolarized membrane potentials and are incompletely inhibited by dihydropyridines. J Neurosci 21:5944–5951. Medline

Yang L, Xu J, Minobe E, Yu L, Feng R, Kameyama A, Yazawa K, Kameyama M (2013) Mechanisms underlying the modulation of L-type Ca^{2+} channel by hydrogen peroxide in guinea pig ventricular myocytes. J Physiol Sci 63:419–426. CrossRef Medline

Yung WH, Häusser MA, Jack JJ (1991) Electrophysiology of dopaminergic and non-dopaminergic neurones of the guinea-pig substantia nigra pars compacta in vitro. J Physiol 436:643–667. CrossRef Medline